Peer-reviewed version available at J. Cardiovasc. Dev. Dis. 2018, 5, 43; doi:10.3390/jcdd5030043

Article

Fenofibrate Induced Cardiac Fibrosis in Mice Deficient in the Protein Quality Control Regulator, CHIP

Saranya Ravi [1], Traci L. Parry [2], Monte S. Willis [2], Pamela Lockyer [1], Cam Patterson [3], James R. Bain [4], Robert D. Stevens [4], Olga R. Ilkayeva [4], Christopher B. Newgard [4], and Jonathan C. Schisler [1,5,*]

[1] McAllister Heart Institute at The University of North Carolina at Chapel Hill, Chapel Hill, NC 27599, USA
[2] Indiana Center for Musculoskeletal Health, University of Indiana School of Medicine, Indianapolis, IN 46202, USA
[3] University of Arkansas for Medical Sciences, Little Rock, AR 72205, USA
[4] Sarah W. Stedman Nutrition and Metabolism Center and Duke Molecular Physiology Institute, Departments of Pharmacology and Cancer Biology and Medicine, Duke University Medical Center, Durham, NC 27701 USA
[5] Department of Pharmacology and Department of Pathology and Lab Medicine, The University of North Carolina at Chapel Hill, Chapel Hill, NC 27599, USA

saranya_ravi@med.unc.edu; tlparry@iu.edu; willisms@iu.edu; plockyer9@gmail.com; CPatters@uams.edu; james.bain@duke.edu; steve018@mc.duke.edu; olga.ilkayeva@duke.edu; newga002@mc.duke.edu
* Correspondence: schisler@unc.edu; Tel.: +1-919-843-8708

Abstract: We previously reported how the loss of CHIP expression (Carboxyl terminus of Hsc70-Interacting Protein) during pressure overload resulted in robust cardiac dysfunction, accompanied by a failure to maintain ATP levels in the face of increased energy demand. In this study, we analyzed the cardiac metabolome after seven days of pressure overload and found an increase in long- and medium-chain fatty acid metabolites in wild-type hearts, a response that was attenuated in mice that lack expression of CHIP (*CHIP*$^{-/-}$). These findings suggest that CHIP may play an essential role in regulating oxidative metabolism, pathways that are regulated in part by the nuclear receptor PPARα (Peroxisome Proliferator-Activated Receptor alpha). Next, we challenged *CHIP*$^{-/-}$ mice with the PPARα agonist, fenofibrate. Surprisingly, treating *CHIP*$^{-/-}$ mice with fenofibrate for five weeks under non-pressure overload conditions resulted in a loss of skeletal muscle mass and a marked increase in cardiac fibrosis, accompanied by a decrease in cardiac function. Isolated *CHIP*$^{-/-}$ cardiac fibroblasts treated with fenofibrate did not increase synthesis of collagen or TGFβ, suggesting that the fibrosis observed in *CHIP*$^{-/-}$ hearts likely depends on signaling from other cell types or circulating factors. In conclusion, in the absence of functional CHIP expression, fenofibrate results in unexpected cardiac pathologies. These findings are particularly relevant to patients harboring loss-of-function mutations in CHIP and are consistent with a prominent role for CHIP in regulating cardiac metabolism.

Keywords: CHIP, metabolism, fenofibrate, fibrosis, metabolomics, pressure overload

1. Introduction

Carboxyl terminus of Hsc70-interacting protein (CHIP, encoded by the gene *STUB1*) is a dual-function enzyme, having both chaperone-related and ubiquitin ligase activities [1]. Coding mutations in *STUB1* cause a multi-organ disease, now identified as SCAR16 (autosomal recessive spinocerebellar ataxia 16, OMIM: 615768), resulting in cerebellar ataxia, cognitive dysfunction, and in some cases, hypogonadism [2,3]. Additionally, CHIP appears to be important for cardiac protein

and metabolic homeostasis, as implicated in models of cardiac hypertrophy and cardiac ischemia-reperfusion injury [4]. For example, CHIP contributed to cardioprotection by preventing cardiomyocyte apoptosis after ischemia [5–7]. Also, over-expression of CHIP prevented cardiac fibrosis and inflammation in an angiotensin II-induced model of hypertension [8], and prevented cardiac myogenesis and pathological hypertrophy under conditions of hyperinsulinemia [9]. In contrast, the genetic deletion of CHIP was found to enhance both physiological and pathological hypertrophy [10,11], and during pressure overload, the loss of CHIP also decreased survival, compromised cardiac function, and reduced metabolic reserves [11]. Metabolic insufficiency in *CHIP*$^{-/-}$ mice following cardiac pressure overload occurred in part due to the inability to increase the activation of 5' AMP-activated protein kinase (AMPK) [11]. CHIP is required for LKB1-mediated phosphorylation and activation of AMPK, through conformational changes to AMPK in the presence of CHIP, that ultimately increase AMPK activity [11]. AMPK is a master metabolic regulator, that senses the cellular energy status through the binding of adenine nucleotides. Increasing AMPK activity promotes fatty-acid and glucose oxidation. These data suggest that targeting other metabolic regulators besides AMPK could potentially blunt the metabolic dysfunction observed in *CHIP*$^{-/-}$ hearts.

Peroxisome Proliferator-Activated Receptor alpha (PPARα) is a nuclear receptor protein that is activated by endogenous ligands such as free fatty acids [12]. Upon activation, PPARα induces the expression of genes involved in fatty acid oxidation, cellular uptake of fatty acids, synthesis of high-density lipoproteins (HDL), apoproteins, and lipoprotein lipase, while suppressing the expression of apolipoprotein C-III [13–16]. Fibrates are PPARα agonists, and this class of pharmaceuticals is commonly used to lower serum triglycerides and increase HDL levels in patients with hyperlipidemia [12]. In this paper, we tested the effect of fenofibrate on cardiac function in *CHIP*$^{-/-}$ mice, with the initial goal of using fibrates to possibly compensate for the metabolic deficiencies when the heart is challenged with a chronic pressure overload. However, in our pharmacological testing of fenofibrate on cardiac function in *CHIP*$^{-/-}$ mice we observed unexpected detrimental effects in skeletal muscle and heart, including decreased cardiac function and increased myocardial fibrosis. Moreover, we did not find a pro-fibrotic phenotype of cardiac fibroblasts isolated from the *CHIP*$^{-/-}$ mice, suggesting that interactions between different cell types and organs are involved in the pathophysiological response to fenofibrate in the absence of functional CHIP expression.

2. Materials and Methods

2.1 Animals

We used CHIP$^{+/-}$ breeding pairs on a 129SvEv background (129S(B6)-*Stub1*^{tm1Cpat}/Mmnc) to generate wild-type (*CHIP*$^{+/+}$), *CHIP*$^{+/-}$, and *CHIP*$^{-/-}$ mice. Animal procedures were approved by the Institutional Animal Care and Use Committee at The University of North Carolina at Chapel Hill and complied with NIH standards for care and use.

2.2 Metabolomic analyses of hearts

Amino acids, acylcarnitines, and organic acids were measured in snap-frozen, powdered mouse heart tissue via stable isotope dilution techniques [17–19]. Samples were equilibrated with a cocktail of internal standards, and de-proteinated by precipitation with methanol. Aliquots of the supernatants were dried, and then esterified with hot, acidic methanol (acyl-carnitines) or n-butanol (amino acids). Data were acquired using a Waters Acquity™ UPLC system equipped with a TQ (triple quadrupole) detector and a data system controlled by the MassLynx 4.1 operating system (Waters, Milford, MA) as described [17,18]. We quantified the concentration of organic acids in samples prepared as described [19], using Trace Ultra GC coupled to ISQ MS operating under Xcalibur 2.2 (Thermo Fisher Scientific, Inc.) [19].

Metabolite concentrations were measured with Metaboanalyst (v3.0) run in the statistical package R (v3.03) [20,21]. Features with more than 50% missing data were removed and the remaining missing values were estimated using KNN (K nearest neighbor). Data were log-

transformed and mean-centered. All metabolites were first evaluated using principal components analysis (PCA). Next, differences in metabolite concentrations were determined using 2-way ANOVA with genotype and surgery as main effects. Metabolites were considered differentially present using a false discovery rate cut off of < 10% at either main effect level or at the interaction level. Raw, processed, and normalized data, along with ANOVA results are available as Supplementary Material. Semi-supervised hierarchical clustering (Euclidean distance and Ward clustering algorithm) was performed on the differential variables and visualized via heatmap.

2.3 ATP and ex vivo oxidation assays.

Cardiac ATP concentrations were measured in whole heart homogenates using the ATP Bioluminescence Assay Kit HS II (Roche) normalized to protein concentration. Oxidation studies from heart homogenates were performed using [1-^{14}C]oleate or [U-^{14}C]glucose as previously described [22,23]. Reactions were terminated by adding 100 µl of 70% perchloric acid, trapping $^{14}CO_2$ in 200 µl of 1 N NaOH and counted in Uniscint BD scintillation solution (National Diagnostics). Acid-soluble metabolites from oleate oxidation were included in total fatty acid oxidation rates and results are expressed as nanomoles of ATP produced per hour per milligram of protein using 129 and 38 moles of ATP per mole of fatty acid or glucose substrate, respectively [24–26].

2.4 Fenofibrate feeding

Mice, 16-18 weeks-of-age (n = 10-15 mice per genotype), were randomized to receive either standard mouse chow (Prolab RMH 3000, Purina LabDiet) or standard chow formulated with 0.05% w/w fenofibrate (Sigma, F6020) as previously described [27]. Mouse chow (fenofibrate and standard sham chow) were administered ad libitum starting on day 1 of the protocol and commencing after five weeks.

2.5 RNA Isolation and Quantitative Polymerase Chain Reaction (qPCR) analysis of gene expression

Total RNA was isolated from mouse liver using the AllPrep DNA/RNA/Protein Mini Kit (Qiagen), and 500 ng of RNA was reverse-transcribed into cDNA using iScript Reverse Transcription Supermix (Bio-Rad, Laboratories, Inc., Hercules, CA, USA). Gene expression assays were performed using Universal Probe (UPL) Assays (Roche) as indicated (**Table 1**) with FastStart Universal Probe Master with Rox (Roche) on the 7900HT instrument (Applied Biosystems). Efficiencies of qPCR reactions (1.9 – 2.1) were confirmed using serial dilution of pooled samples. Three biological replicates were used in triplicate technical replicates per gene. Relative mRNA levels were calculated using the delta Cq method: data was centered using the geometric mean of all control chow samples and 18S ribosomal RNA levels (4310893E, Applied Biosystems) to normalize loading.

Table 1. Probes and primers used for qPCR analysis.

Gene	UPL probe	Sense (5′ – 3′)	Anti-sense (5′ – 3′)
Acox1	#45	gcgccagtctgaaatcaag	actgctgcgtctgaaaatcc
Cpt1a	#109	gctgtcaaagataccgtgagc	tctccctccttcatcagtgg
Cpt2	#71	ccaaagaagcagcgatgg	tagagctcaggcagggtga
Pdk4	#22	ctgcctgaccgcttagtga	cttctgggctcttctcatgg
Ucp2	#2	acagccttctgcactcctg	ggctgggagacgaaacact
Ppard	#11	atgggggaccagaacacac	ggaggaattctgggagaggt
Ppargc1a	#6	cagtcgcaacatgctcaag	tggggtcatttggtgactct
Ppara	#41	cacgcatgtgaaggctgtaa	cagctccgatcacacttgtc

2.6 Measurement of Blood Chemistry

After the animals were euthanized, blood was collected in tubes containing EDTA/citrate. The blood was then centrifuged at 3000 × *g* for three minutes to separate the plasma from the red blood

cells. Levels of triglyceride, total cholesterol, HDL, glucose, creatine kinase and creatine kinase-MB were measured by the Animal Histopathology and Lab Medicine Core at The University of North Carolina at Chapel Hill. Low-density lipoprotein (LDL) was calculated using the formula: total cholesterol – HDL – (triglycerides/5).

2.7 Echocardiography

The mice underwent conscious echocardiography using the Vevo 770 ultrasound microimaging system (VisualSonics, Inc., Toronto, Canada) as previously described [28–30].

2.8 Histology and transmission electron microscopy

For histological assessment, mouse hearts were perfused with 4% paraformaldehyde, embedded in paraffin, and sectioned into 5-micron sections. Heart sections were stained with either H&E or Masson's trichrome staining. Whole slides were imaged using the Aperio Scanscope and analyzed using Aperio Imagescope software (v10.0.36.1805, Aperio Technologies). Fibrosis was determined using the Positive Pixel Count Algorithm to analyze Masson's trichrome-stained four-chamber sections (n= 3/mouse), hue value=0.66 (blue), and hue width=0.1 (detection threshold above background white) as described [11,27], and the amount of fibrosis was calculated as the weighted average collagen per total tissue area. Myocyte area was determined using NIH ImageJ (v1.38), based on photomicrographs of a standard graticule ruler. Hearts apices were fixed and imaged using a EM910 transmission electron microscope (LEO Electron Microscopy) as described previously [31].

2.9 Fibroblast isolation

Hearts were isolated from mice at eight weeks of age, and rinsed in PBS before cutting them into approximately one mm^3 sections. Two hearts per genotype were placed in 10 cm^2 dishes with 2 ml RPMI-1640 containing 20% FBS and insulin (10 μg/ml). The tissue remained undisturbed for three hours, after which it the tissue was supplemented with an additional 8 ml of media. Media were replaced every two days, and after three weeks the fibroblasts were used for downstream analyses.

2.10 Immunoblot analysis

8E6 fibroblasts were plated per well on 6-well plates, serum-starved overnight, and then treated with either vehicle or fenofibrate (20 μM) for 24 h. Supernatant was collected, and the cells were washed in PBS, collected, and lysed in RIPA buffer. Supernatant samples were concentrated by using the Amicon Ultra Centrifugal Filter Unit with a 10kDa cutoff (EMD Millipore, UFC801008). Media (2 ml) were concentrated to a volume of 65 μl and mixed with 4x Laemmli sample buffer before boiling. Similarly, 15 μg of lysates were mixed with 4x Laemmli sample buffer and boiled. Samples were separated on 4-15% stain-free gels (BioRad) and transferred onto PVDF before probing with antibodies against pan-collagen (MMCRI, Vli42), TGFβ (Cell Signaling, 3711S) and CHIP (Abcam, ab134064). Total protein per lane was quantified by stain-free quantification of the total amount of protein present on the membrane in each lane [32–34].

3. Results

3.1 Role of CHIP in fatty acid metabolism

We previously reported a surprisingly low AMPK activity after one week of pressure overload in *CHIP*$^{-/-}$ mice, despite the increase in metabolic demand [11]. AMPK can drive oxidative metabolism, including fatty acid and glucose oxidation. We measured differences in metabolites from wild-type and *CHIP*$^{-/-}$ hearts in the context of pressure overload by trans-aortic banding (TAB) for one week. Principal components analysis of 74 acylcarnitine, amino acid, and organic acid metabolites revealed distinct differences in the TAB conditions comparing wild-type and *CHIP*$^{-/-}$ hearts (**Figure 1a**). We identified differential metabolites via 2-way ANOVA, including an increase in the carnitine esters of several medium-chain (MC) and long-chain (LC) fatty acids as well as α-ketoglutarate

Preprints (www.preprints.org) | NOT PEER-REVIEWED | Posted: 9 July 2018 doi:10.20944/preprints201807.0137.v1

Peer-reviewed version available at J. Cardiovasc. Dev. Dis. 2018, 5, 43; doi:10.3390/jcdd5030043

(**Figure 1b**). The majority of the differences we observed were manifest in increases in MC and LC acylcarnitines with pressure overload in wild-type hearts, an effect that was attenuated in *CHIP*$^{-/-}$ hearts. These data suggest that pressure overload in wild-type hearts results in specific changes to oxidative metabolic flux that are distinct from those found in *CHIP*$^{-/-}$ hearts. Using fresh cardiac homogenates, we tested oxidative metabolism in these same conditions. As expected, pressure overload resulted in a compensatory increase in ATP production, mostly from an increase in fatty acid oxidation (**Figure 1c**), consistent with our metabolite data (**Figure 1b**). Remarkably, in samples from pressure-overloaded *CHIP*$^{-/-}$ hearts, there was a dramatic drop in glucose oxidation and unlike wild-type hearts, no increase in fatty acid oxidation, resulting in an overall decrease in oxidative ATP generation. We also measured steady-state ATP levels (**Figure 1d**) and observed similar patterns to our calculated ATP values (**Figure 1e**), again highlighting the disparity between wild-type and *CHIP*$^{-/-}$ hearts after pressure overload. Therefore, we conducted a pilot study to determine the effect of treating *CHIP*$^{-/-}$ mice with fenofibrate as a possible approach for rescuing the metabolic defect seen during pressure overload.

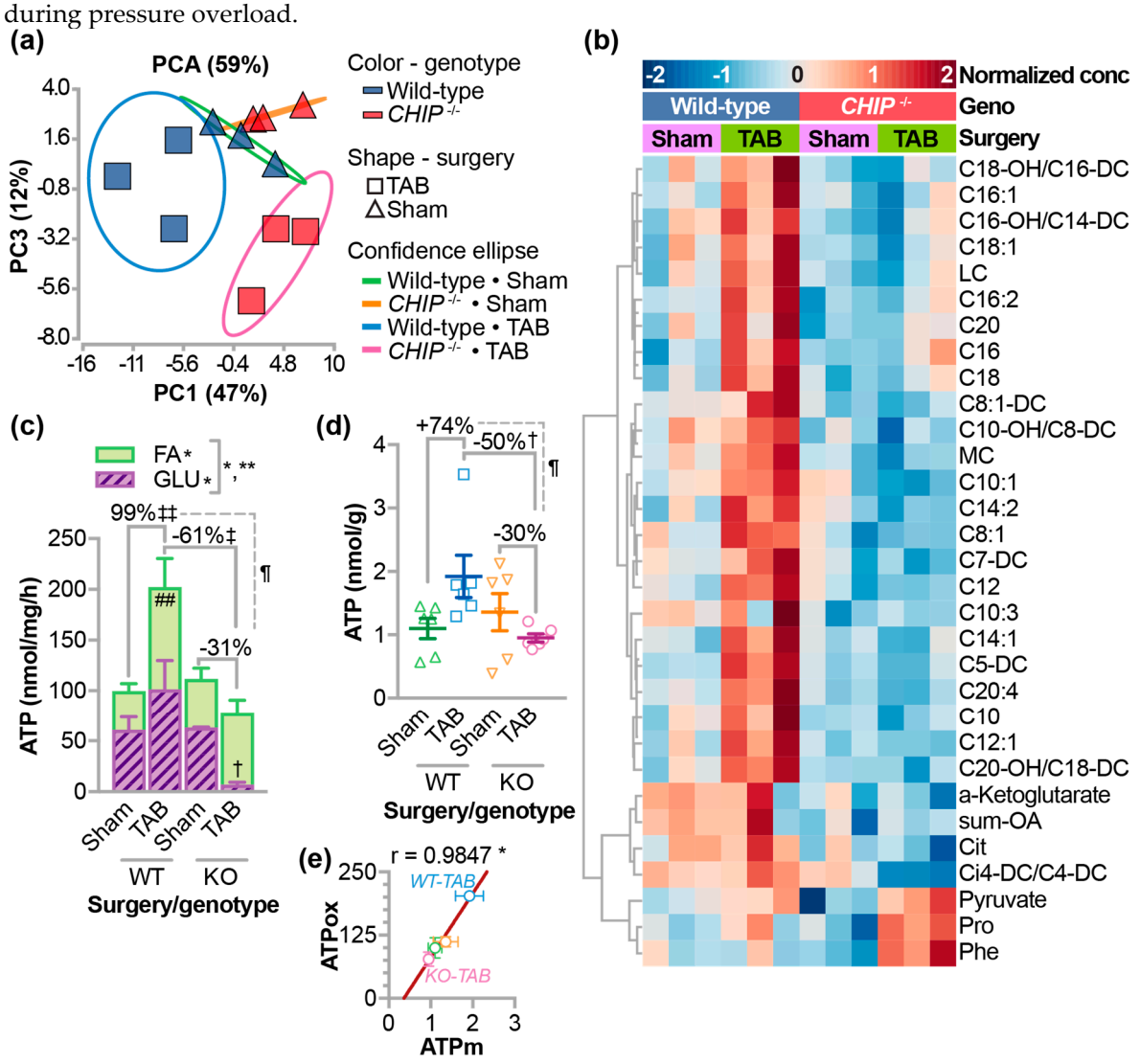

Figure 1. Effects of pressure overload on metabolism in *CHIP*$^{-/-}$ hearts. Metabolomic analysis of whole hearts isolated from wild-type or *CHIP*$^{-/-}$ mice one week after a sham surgery or trans-aortic banding (TAB) were analyzed using **(a)** principal component analysis (PCA) and **(b)** 2-way ANOVA. Variances captured by the first and third principal components (PC) are shown. Differential metabolites via ANOVA (FDR < 10%) were clustered and represented by heatmap. **(c)** *Ex-vivo* oxidative ATP generation rates in mouse heart homogenates represented by the mean ± SEM from three biological replicates using either fatty acid (open bars) or glucose (hashed bars) as substrate. 2-way ANOVA for glucose oxidation: * $p < 0.05$ of genotype main effect and interaction between genotype and surgery, post-test: † $p < 0.05$ glucose oxidation in wild-type vs *CHIP*$^{-/-}$ after one week of

TAB. 2-way ANOVA for fatty acid oxidation, * $p < 0.05$ on surgery main effect. 2-way ANOVA for total ATP, * $p < 0.05$ on surgery main effect, ** $p < 0.01$ on genotype main effect and interaction, post-test: ‡‡ $p < 0.01$ total ATP in wild-type sham vs TAB mice, post-test:, ‡ $p < 0.05$ total ATP in wild-type vs *CHIP*$^{-/-}$ after one week of TAB, and the surgery-dependent percent change in ATP production rates (TAB vs sham) in wild-type vs *CHIP*$^{-/-}$ was significant at $p = 0.039$ ¶. (**d**) Steady-state ATP levels in mouse hearts represented by the mean ± SEM from six biological replicates. 2-way ANOVA interaction of main effects $p = 0.0177$, post-test: † $p < 0.05$ in wild-type vs *CHIP*$^{-/-}$ at one week of TAB, and the surgery-dependent percent change in ATP levels (TAB vs sham) in wild-type vs *CHIP*$^{-/-}$ was significant at $p = 0.034$ ¶. **(e)** Pearson correlation analysis of ATP determined by ex vivo oxidization rates (ATPox) or measured steady-state ATP levels (ATPm) * $p = 0.0153$.

3.2 Fenofibrate activated PPARα target genes in the liver

Since the loss of CHIP expression appears to confer a loss of metabolic flexibility, we initiated a study to challenge *CHIP*$^{-/-}$ mice with fenofibrate, a PPARα agonist, to determine the effect of a drug that is known to stimulate oxidative metabolism. Mice were administered fenofibrate, by incorporating the drug into the chow. Cardiac function was evaluated by echocardiography at two and five weeks, and changes in gene expression, blood chemistry and body weights were assessed after the five-week feeding period (**Figure 2a**). To demonstrate that the fenofibrate dose stimulated PPARα activity, we first analyzed known liver target genes of PPARα using quantitative PCR (qPCR). As expected, fenofibrate increased expression of *Cpt1a* (Carnitine palmitoyltransferase 1a), *Cpt2* (Carnitine palmitoyltransferase 2), *Ucp2* (Uncoupling protein 2), *Acox1* (Acyl-CoA oxidase 1) and *Pdk4* (Pyruvate dehydrogenase kinase 4) to similar levels in both wild-type and *CHIP*$^{-/-}$ mice (**Figure 2b**) [35–37]. However, there were no changes in *Ppargc1a* (Pparg coactivator 1 alpha), *Ppara*, and *Ppard* expression, suggesting no increases in mitochondrial biogenesis (**Figure 2b**). Previous reports demonstrate that fenofibrate increases liver weight in mice [37,38], and in fact, we observed similar increases in liver weights in both wild-type and *CHIP*$^{-/-}$ mice that were fed fenofibrate chow (**Figure 2c**). Together, these data suggest that the transcriptional and phenotypic response to fenofibrate in the liver, the primary target organ of fibrates, is not affected by the loss of CHIP expression.

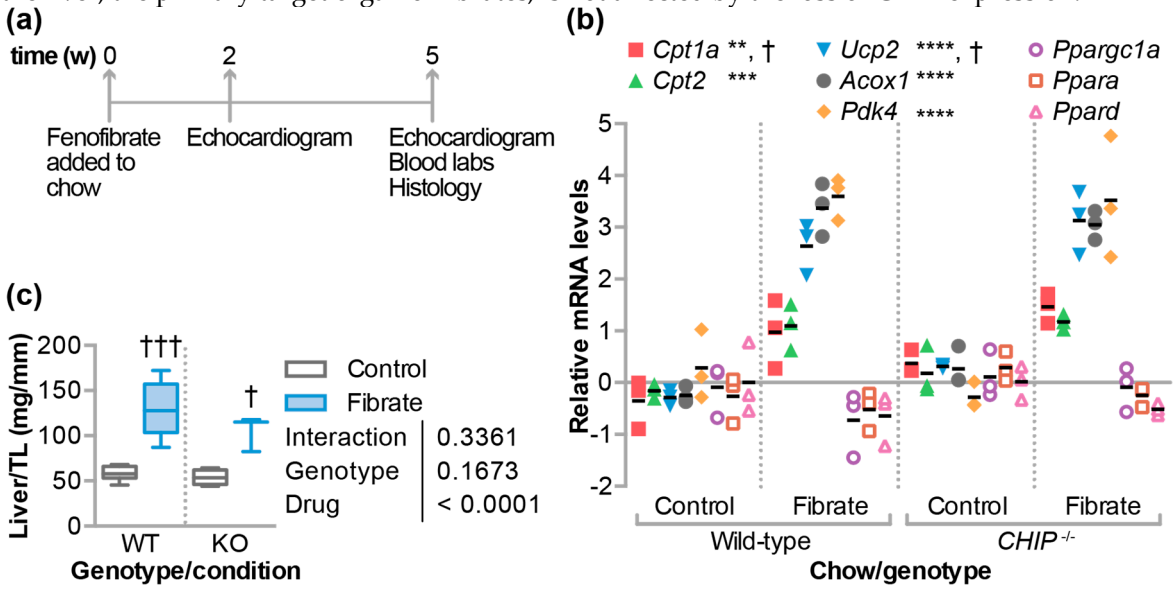

Figure 2. The effect of fenofibrate on liver. (a) Experimental design used in the study. **(b)** Quantitative PCR analysis of gene expression in livers from either wild-type (WT) or *CHIP*$^{-/-}$ (KO) mice fed control or fenofibrate chow, represented by scatter plot (n = 3 animals per condition): **, ***, *** indicate $p < 0.01$, 0.001, 0.0001 or † $p < 0.05$ on the main effect of chow or genotype, respectively, via 2-way ANOVA. **(c)** Liver weight normalized to tibia length (TL) represented by boxplot (n = 4-6 animals per condition). Results of 2-way ANOVA are provided, Tukey's post-test: † and †† indicate $p < 0.05$ and 0.01 comparing control vs. fibrate conditions.

Preprints (www.preprints.org) | NOT PEER-REVIEWED | Posted: 9 July 2018 doi:10.20944/preprints201807.0137.v1

Peer-reviewed version available at J. Cardiovasc. Dev. Dis. 2018, 5, 43; doi:10.3390/jcdd5030043

3.3 Fenofibrate altered circulating cholesterol in wild-type, but not CHIP$^{-/-}$ mice

Fibrates are primarily used to treat hypercholesterolemia and hypertriglyceridemia, and although we are not studying models of hyperlipidemia, we investigated the impact of fibrates on lipid profiles in our particular models. As expected, there were no changes in triglyceride levels with respect to genotype or chow (**Figure 3a**). Paradoxically, we, and others, observed that fenofibrate increases levels of total cholesterol in mice on standard chow (non-Western) diets [27,39]. Here we observed that fenofibrate led to a 58% increase in total cholesterol levels in WT mice, an effect that was ablated in *CHIP*$^{-/-}$ mice (**Figure 3b**). The increase in total cholesterol was comprised of similar increases in both high-density lipoprotein cholesterol (HDL-c) and low-density lipoprotein cholesterol (LDL-c) in wild-type mice treated with fenofibrate, whereas these levels did not change in *CHIP*$^{-/-}$ mice (**Figure 3c, 3d**).

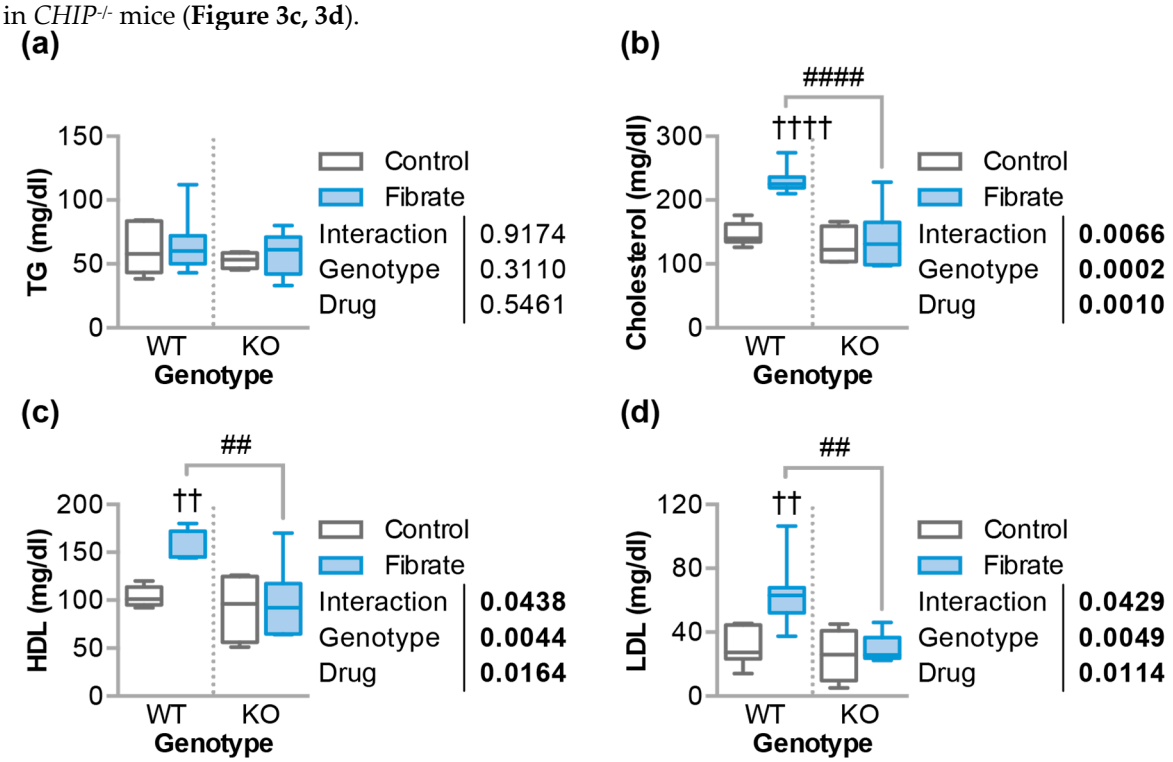

Figure 3. Fenofibrate effects on circulating lipid levels. (a) Triglycerides (TG), **(b)** total cholesterol , **(c)** HDL cholesterol, and **(d)** LDL cholesterol, in either wild-type (WT) or *CHIP*$^{-/-}$ (KO) mice fed control or fenofibrate chow, represented by boxplot (n = 4-8 animals per condition). Results of 2-way ANOVA are provided, Tukey's post-test: †† and †††† indicate $p < 0.01$ and 0.0001 comparing control vs. fibrate conditions; ## and #### indicate $p < 0.01$ and 0.0001 comparing WT vs. KO conditions.

3.4 Differential effects of fenofibrate on skeletal muscle

Fenofibrate a did not alter body weights of either wild-type or *CHIP*$^{-/-}$ mice (normalized to tibia length), nor were there baseline differences between wild-type or *CHIP*$^{-/-}$ mice. However, after five weeks of fenofibrate, *CHIP*$^{-/-}$ mice were 23% lighter than wild-type mice (**Figure 4a**). *CHIP*$^{-/-}$ mice trended towards higher fasting blood glucose levels compared to wild-type mice, however, fenofibrate did not affect fasting blood glucose in either wild-type or *CHIP*$^{-/-}$ mice (**Figure 4b**). Given the known defects in *CHIP*$^{-/-}$ skeletal muscle [40], we measured creatine kinase (CK) and creatine kinase-MB (CKMB), enzymes that are indicators of muscle damage. Interestingly, 2-way ANOVA indicated an interaction between genotype and drug treatment, with higher CK and CKMB levels in *CHIP*$^{-/-}$ mice treated with fenofibrate (**Figure 4c, 4d**), suggesting that either skeletal or cardiac muscle may be negatively affected by fenofibrate in the absence of CHIP expression. Therefore, we measured various muscle weights and found that the tibialis anterior, soleus, and gastrocnemius muscles, on average, were all reduced in *CHIP*$^{-/-}$ mice; moreover, fenofibrate led to muscle atrophy in *CHIP*$^{-/-}$ mice, an effect not observed in wild-type mice (**Figure 4e, 4f, 4g**). We did not observe any changes in heart

weight (**Figure 4h**), suggesting that the increase in muscle enzymes seen in *CHIP*$^{-/-}$ mice treated with fenofibrate is likely indicative of skeletal muscle atrophy. We previously described accumulation of lamellar bodies in the gastrocnemius muscle in *CHIP*$^{-/-}$ mice. Fenofibrate did not appear to affect the appearance of these structures, however, in both wild-type and *CHIP*$^{-/-}$ mice on fenofibrate chow we observed glycogen accumulation throughout the sarcomere predominantly in the I-band and the sarcoplasm (**Figure 4i, 4j**).

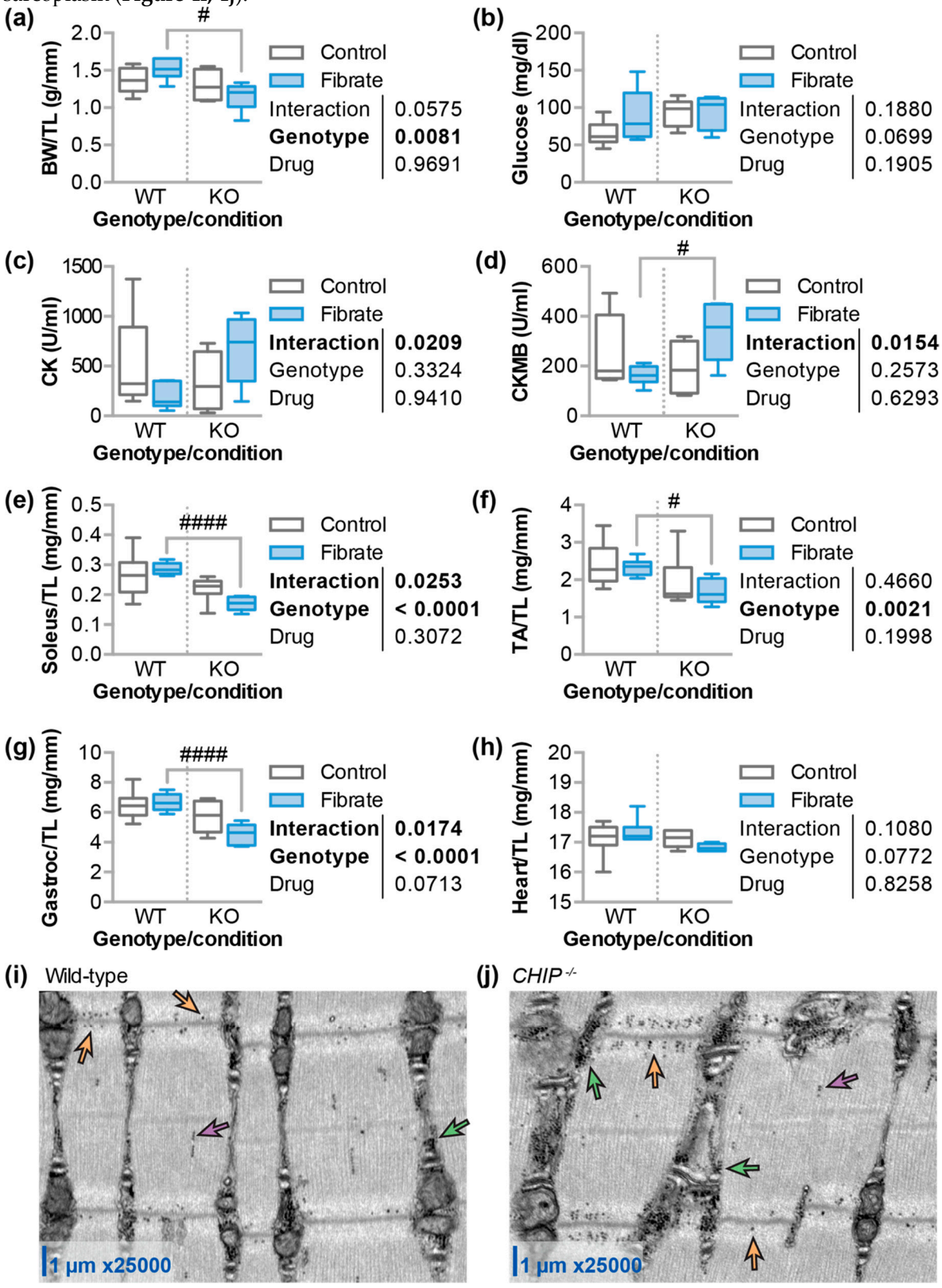

Figure 4. Fenofibrate effects on body weight, glucose levels, and muscle. (a) Body weight (BW) normalized by tibia length (TL), circulating levels of **(b)** glucose , **(c)** creatine kinase (CK) or **(d)**

creatine kinase MB (CKMB), and weights of **(e)** soleus, **(f)** tibialis anterior **(g)** gastrocnemius (gastroc), and **(h)** heart, normalized by TL, in either wild-type (WT) or *CHIP*$^{-/-}$ (KO) mice fed control or fenofibrate chow, represented by boxplot (n = 4-8 animals per condition). Results of 2-way ANOVA are provided, Tukey's post-test: #, ###, and #### indicate $p < 0.05$, 0.001, and 0.0001 comparing WT vs. KO conditions. Transmission electron micrographs of gastrocnemius muscle sarcomeres from **(i)** wild-type and **(j)** *CHIP*$^{-/-}$ mice. Glycogen can be seen as small, dense round objects, highlighted by arrows, found in the I-band (orange), A-band (purple), and sarcoplasm (green).

Table 1. Echocardiogram results of study mice. Left ventricular dimension data obtained via conscious echocardiography. When applicable, measurements reported at diastole or systole (d or s respectively); g, grams; bpm, beats per minute; mm, millimeters; IVS, interventricular septum; LVID, left ventricular internal diameter; LVPW, left ventricular posterior wall; LV Vol, left ventricle volume; EF, ejection fraction. Results of 2-way ANOVA on the main effects (genotype, Geno; metformin, Drug) and the interaction (Inter) are indicated, Tukey's post-test: *** $p < 0.001$ comparing 2 w vs 0 w; #, ##, and ### indicate $p < 0.05$, 0.01 and 0.001 comparing WT vs. KO at 2 w; † and ††† $p < 0.05$ and 0.001 comparing 5 w vs 2 w.

			Genotype	Wild-type			*CHIP*$^{-/-}$		
Parameter	**Effect**	***p***	**weeks**	**0**	**2**	**5**	**0**	**2**	**5**
HR (bpm)	Inter	0.915		600.7 ± 23.8	660.3 ± 17.9	640.5 ± 17.8	602.0 ± 28.0	645.3 ± 26.5	625.5 ± 17.5
	Geno	0.085							
	Drug	0.604							
IVS;d (mm)	Inter	0.0004		1.07 ± 0.02	0.99 ± 0.02	1.11 ± 0.03	1.04 ± 0.02	1.3 ± 0.5***,###	1.04 ± 0.06†††
	Geno	0.0027							
	Drug	0.146							
LVID;d (mm)	Inter	0.699		3.50 ± 0.16	3.09 ± 0.14	3.35 ± 0.10	3.26 ± 0.14	3.09 ± 0.24	3.3 ± 0.13
	Geno	0.137							
	Drug	0.425							
LVPW;d (mm)	Inter	0.017		1.04 ± 0.03	1.02 ± 0.01	1.09 ± 0.04	1.00 ± 0.042	1.17 ± 0.07	0.99 ± 0.05†
	Geno	0.143							
	Drug	0.948							
IVS;s (mm)	Inter	0.0029		1.75 ± 0.06	1.69 ± 0.05	1.86 ± 0.05	1.74 ± 0.07	2.02 ± 0.06##	1.69 ± 0.09†
	Geno	0.247							
	Drug	0.398							
LVID;s (mm)	Inter	0.263		1.61 ± 0.08	1.39 ± 0.09	1.43 ± 0.05	1.49 ± 0.09	1.51 ± 0.20	1.63 ± 1.11
	Geno	0.572							
	Drug	0.426							
LVPW;s (mm)	Inter	0.473		1.59 ± 0.04	1.57 ± 0.08	1.68 ± 0.07	1.53 ± 0.05	1.53 ± 0.06	1.5 ± 0.05
	Geno	0.782							
	Drug	0.068							
LV Vol;d (µl)	Inter	0.617		51.92 ± 5.57	38.30 ± 4.02	46.04 ± 3.07	43.46 ± 4.40	38.84 ± 7.82	44.86 ± 4.39
	Geno	0.161							
	Drug	0.447							
LV Vol;s (µl)	Inter	0.254		7.46 ± 0.91	5.13 ± 0.88	5.51 ± 0.51	6.16 ± 1.03	6.80 ± 2.42	7.89 ± 1.20
	Geno	0.723							
	Drug	0.329							
LV Mass (mg)	Inter	0.0039		140.18 ± 7.13	109.95 ± 6.87	140.74 ± 8.32	120.86 ± 11.18	150.08 ± 8.21#	122.31 ± 11.08
	Geno	0.986							
	Drug	0.917							
EF (%)	Inter	0.087		85.42 ± 0.75	86.89 ± 1.0	87.78 ± 1.12	86.05 ± 0.86	83.84 ± 2.40	82.7 ± 1.71
	Geno	0.915							
	Drug	0.021							

Preprints (www.preprints.org) | NOT PEER-REVIEWED | Posted: 9 July 2018 doi:10.20944/preprints201807.0137.v1

Peer-reviewed version available at J. Cardiovasc. Dev. Dis. 2018, 5, 43; doi:10.3390/jcdd5030043

3.5 Fenofibrate decreased cardiac function and increased fibrosis in CHIP$^{-/-}$ mice

We next measured cardiac function at two and five weeks after fenofibrate treatment using conscious echocardiography (**Table 1**). There were changes at the two-week time point in *CHIP*$^{-/-}$ mice, notably an increase in interventricular septum size in both diastole and systole, and calculated left-ventricular (LV) mass, suggestive of LV wall thickening, however, these changes resolved at the five-week time point. Fenofibrate also caused a modest 11% decrease in cardiac function after five weeks, as measured by fractional shortening (**Figure 5a**). We analyzed ventricle tissue to determine cardiomyocyte surface area and fibrosis using histochemical approaches developed in our lab [11,27] (**Figure 5b**). On average, *CHIP*$^{-/-}$ mice had larger cardiomyocyte surface area, but these parameters were not changed with fenofibrate. In contrast, we observed increased cardiac fibrosis in *CHIP*$^{-/-}$ mice after fenofibrate treatment (**Figure 5d**), suggesting that fenofibrate causes pathophysiological cardiac remodeling in the absence of CHIP.

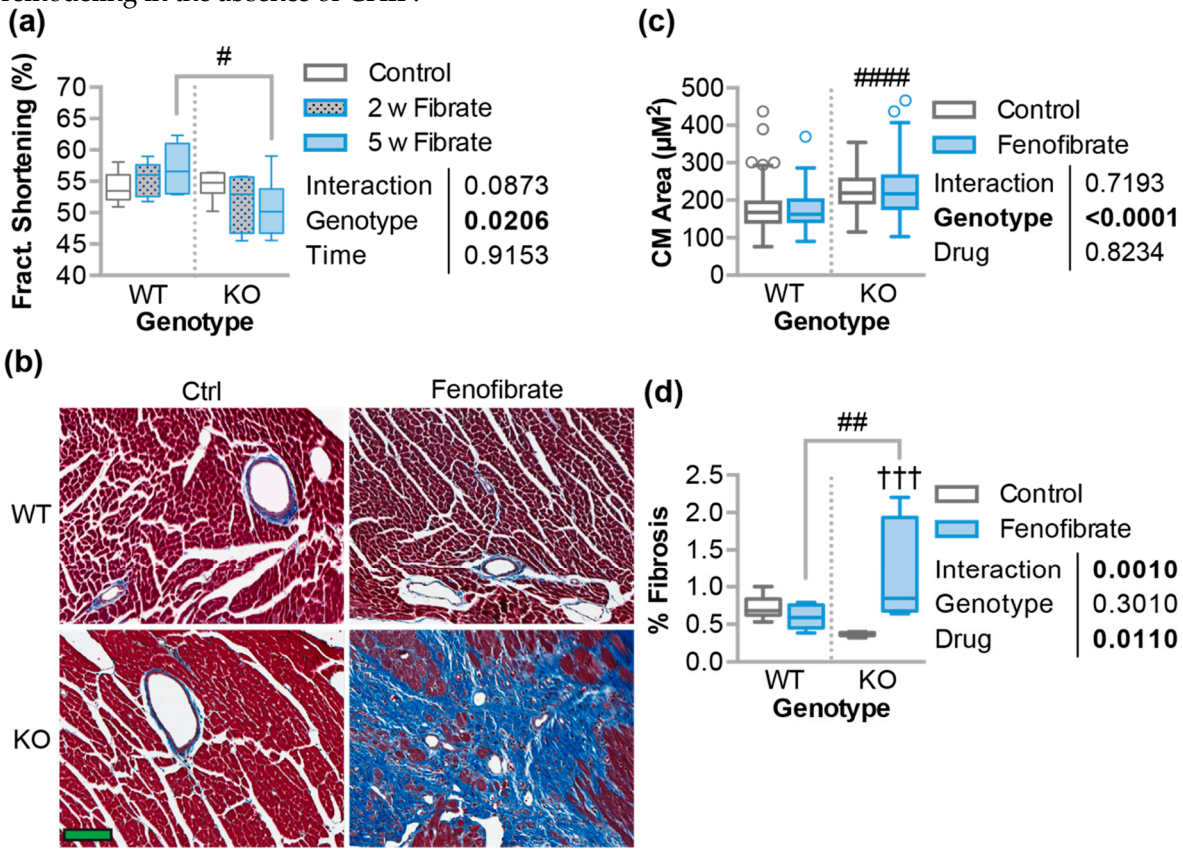

Figure 5. Changes in cardiac function and structure due to fenofibrate. (a) Fractional (fract.) shortening over the time course of the study, represented by boxplot (n = 4-6 animals per condition). Results of 2-way ANOVA are provided, Tukey's post-test: # $p < 0.05$ comparing wild-type (WT) vs. *CHIP*$^{-/-}$ (KO) conditions. **(b)** Micrographs of Masson's trichrome staining of heart sections, scale bar represents 100 microns. **(c)** Cardiomyocyte area and **(d)** the percentage of fibrotic cardiac tissue, represented by boxplot (n = 3 animals represented by four sections per animal). Results of 2-way ANOVA are provided, Tukey's post-test: ## and #### $p < 0.01$ and 0.0001 comparing WT vs. KO conditions; ††† $p < 0.001$ control vs. fibrate conditions.

3.6 The effect of fenofibrate on collagen secretion from primary cardiac fibroblasts and on mitochondrial ultrastructure in the cardiac sarcomere

One of the primary roles of fibroblasts is the production of extracellular matrix to support tissue structure, both in health and disease. Given the increase in fibrosis seen in hearts of *CHIP*$^{-/-}$ mice treated with fenofibrate, we tested our hypothesis that fenofibrate stimulates collagen expression in cardiac fibroblasts isolated from *CHIP*$^{-/-}$ hearts. Primary cardic fibroblasts were treated with fenofibrate for 24 h, after which the supernatant and cell lysates were analyzed via immunoblot

analysis for collagen and TGFβ. Surprisingly, we did not observe any differences in collagen levels from cells isolated from *CHIP*$^{-/-}$ mice compared to wild-type, or in the presence of fenofibrate (**Figure 6a**). TGFβ, which induces multiple pro-fibrotic genes, was also unchanged in response to fenofibrate treatment in both wild-type and *CHIP*$^{-/-}$ fibroblasts (**Figure 6a**). Although we did not observe any structural differences in unstressed *CHIP*$^{-/-}$ hearts [11], we found that compared to wild-type sarcomeres (**Figure 6b**), the ultrastructure of cardiac sarcomeres in *CHIP*$^{-/-}$ mice treated with fenofibrate had various regions with expanded sarcoplasmic reticulum, as well as changes in mitochondrial morphology, most notably decreased cristae density (**Figure 6c**).

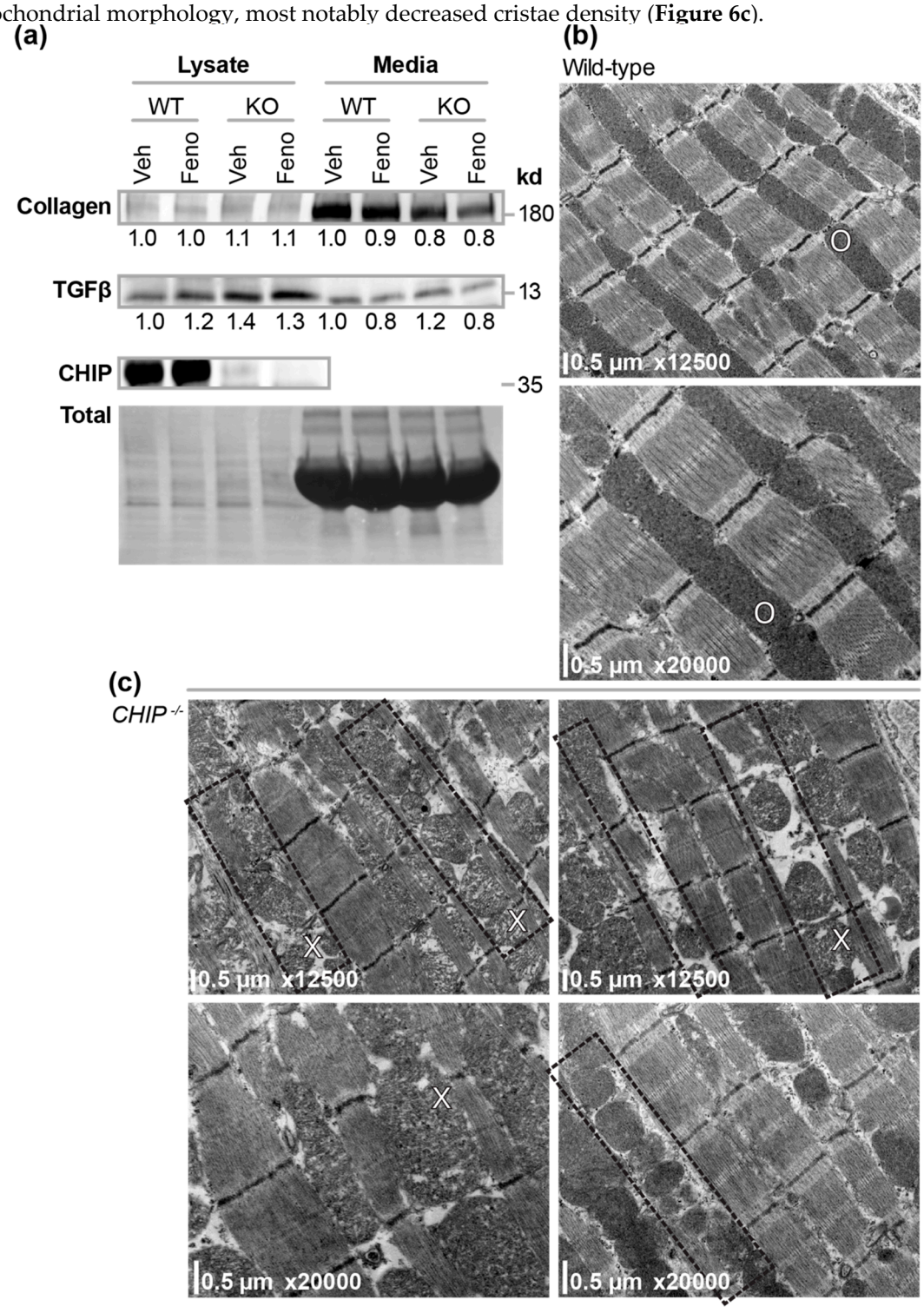

Figure 6. Effect of fenofibrate on cardiac fibroblasts and mitochondrial ultrastructure in the absence of CHIP expression. (a) Representative immunoblot of collagen, TGFβ, and CHIP either from cellular lysates or conditioned medium of cardiac fibroblasts isolated from wild-type (WT) or

CHIP$^{-/-}$ (KO) hearts and subsequently treated with vehicle or 20 μM fenofibrate for 24 hrs. Densitometry analysis is indicated, no changes were observed ($p > 0.05$). Transmission electron micrographs of left ventricle tissue from **(b)** wild-type and **(c)** *CHIP*$^{-/-}$ mice. Expanded sarcoplasm regions are observed throughout *CHIP*$^{-/-}$ hearts (outlined in boxes). Alterations in mitochondria were also observed in *CHIP*$^{-/-}$ hearts (X) compared to wild-type hearts (O).

4. Discussion

Pressure overload and the subsequent pathological remodeling in the heart is associated with changes in cardiac metabolism [41–43]. In the initial compensatory phase of pressure overload, the heart adapts to the increased demand and can maintain cardiac output; however, over time, if the stress is not relieved, this adaptation turns to maladaptation and eventual heart failure. In our mouse model of pressure overload, the initial adaptation is exemplified after one week, as wild-type hearts maintain function in part due to compensatory cardiomyocyte hypertrophy [11]. Deletion of CHIP in mice results in the inability to meet cardiac energy demands during pressure overload, leading to robust cardiac hypertrophy and impaired cardiac function [11], perhaps reflective of the metabolic inflexibility of *CHIP*$^{-/-}$ mice to pathological stressors. We used metabolomics (**Figure 1a**) to identify changes that occur during this adaptive phase in both wild-type and *CHIP*$^{-/-}$ mice. We observed an increase in long- and medium-chain acylcarnitines (**Figure 1b**) that was accompanied by an increase in fatty acid oxidation and total oxidation (**Figure 1c**) as well as increased ATP levels (**Figure 1d, 1e**), consistent with our previous report [11]. These effects were attenuated in *CHIP*$^{-/-}$ mice (**Figure 1b, 1c, 1d, 1e**) consistent with our hypothesis that CHIP is necessary for cardiac metabolic flexibility. We decided to test the effect of stimulating oxidative metabolism pharmacologically using the PPARα agonist, fenofibrate, in *CHIP*$^{-/-}$ mice (**Figure 2a**). Unexpectedly, treating *CHIP*$^{-/-}$ animals with fenofibrate decreased cardiac function (**Figure 5a**) and induced cardiac fibrosis (**Figure 5b, 5d**). Interestingly, collagen expression and secretion were not increased in isolated cardiac fibroblasts from *CHIP*$^{-/-}$ mice, nor did fenofibrate affect collagen levels (**Figure 6a**), suggesting that integrated signaling from within the heart or other organ systems likely contributes to the phenotype observed in our study. Changes in mitochondrial ultrastructure were observed in *CHIP*$^{-/-}$ mice treated with fenofibrate, including a decrease in cristae density. Fenofibrate can induce changes in hepatic mitochondria in rodents, canines, and humans [44,45] and mitochondrial impairment is thought to mediate the toxicity of fibrates as well as statins and thiazolidinediones [46]; therefore, the cardiac effects seen in *CHIP*$^{-/-}$ mice treated with fenofibrate may be a result of impaired mitochondrial function.

PPARα target genes in the heart are poorly defined; however, we found that the expression of hepatic genes known to be responsive to PPARα agonists were regulated to a similar extent in wild-type and *CHIP*$^{-/-}$ animals, suggesting that CHIP expression was not necessary for PPARα-mediated gene transcription. Likewise, we saw an equivalent increase in liver mass with fenofibrate in mice of either genotype (**Figure 2c**), as shown previously in multiple mouse lines [36,37,47]. In contrast, fenofibrate had differential effects on circulating lipids when comparing wild-type and *CHIP*$^{-/-}$ animals. As seen in other mouse models [27,39], fenofibrate increased total, HDL-, and LDL-cholesterol levels in wild-type mice, a response that was entirely absent in *CHIP*$^{-/-}$ mice (**Figure 3b, 3c, 3d**). We also found that fenofibrate had deleterious effects on skeletal muscle in *CHIP*$^{-/-}$ mice, notably an increase in muscle proteins in the circulation (**Figure 4c, 4d**) and a decrease in muscle mass (**Figure 4e, 4f, 4g**).

Published findings present a mixed picture regarding the effects of fenofibrate on cardiac function in animal models--the majority of studies demonstrate a protective role of fenofibrate on cardiac function, by decreasing the degree of cardiac remodeling and fibrosis, as seen in mouse, rat and canine models [48–53]. In contrast, in mouse models with altered cardiac metabolism, fenofibrate appears to mediate pathophysiological responses. For example, fenofibrate promoted cardiac hypertrophy in mice lacking MuRF1 expression, however there were no changes in fibrosis, ejection fraction, of fractional shortening [27]. Likewise, fenofibrate treatment increased cardiac hypertrophy and fibrosis, along with a decrease in fractional shortening during pressure overload in PPARα

deficient mice [54]. These later studies, combined with our results, highlight deleterious consequences of fibrate treatment in the context of altered cardiac metabolism. Clinically, there are reported incidences of fenofibrate-related side effects, including liver fibrosis [55] and nephrotoxicity [56]; moreover, these findings may be particularly relevant in patients with MuRF1 or CHIP loss-of-function mutations [2,3,57,58]

Cardiac fibroblasts are the primary effector cells involved in cardiac fibrosis through the deposition of extracellular matrix [59]. While previous studies examined whole heart sections to detect fibrosis in fenofibrate models [48–50,54], the specific action of fenofibrates on cardiac fibroblasts in producing extracellular matrix components has not been studied in detail. Much to our surprise, treating *CHIP*$^{-/-}$ cardiac fibroblasts with fenofibrate did not alter collagen or TGFβ expression (**Figure 6a**). Crosstalk between fibroblasts and cardiomyocytes through exosomes, cell interactions, and paracrine mediators is vital in mediating fibrotic stimuli [60–64]. Absence of communication between the cardiomyocyte other cell types in the heart, as well as distant organs, could explain the lack of an enhanced fibrotic response in the isolated fibroblasts from the *CHIP*$^{-/-}$ hearts.

Future studies will focus on trying to understand the metabolic changes accompanying fenofibrate treatment of *CHIP*$^{-/-}$ mice and whether they differ from those in wild-type animals, including deleterious effects on cardiac mitochondria. Additionally, defining the integrated stimuli that induces the pro-fibrotic phenotype of *CHIP*$^{-/-}$ fibroblasts will help to elucidate the sensitization caused by the loss of CHIP function.

Supplementary Materials: The metabolomics datasets are available online at the Carolina Digital Repository: doi.org/10.17615/C6WM1F.

Acknowledgments: We thank members of the Schisler Laboratory for critical review of the manuscript; the Willis, Jensen, McLean, and Stouffer Laboratories for support; and The McAllister Heart Institute and Cardiology administration teams.

Author Contributions: Conceptualization, J.C.S. and C.P.; Methodology, M.S.W., J.R.B., R.D.S., O.R.I., C.B.N., and J.C.S.; Formal Analysis, S.R., T.L.P., J.R.B, and J.C.S.; Investigation, S.R., P.L., M.S.W., J.R.B., R.D.S., and J.C.S.; Writing-Original Draft Preparation, S.R.; Writing-Review & Editing, S.R., T.L.P., M.S.W., J.R.B., C.B.N., and J.C.S.; Visualization, S.R. and J.C.S.; Supervision, M.S.W, C.P., C.B.N., and J.C.S.; Project Administration, T.L.P. and P.L..; Funding Acquisition, C.P.

Funding: This research was supported by the National Institutes of Health (NIH) grants R01GM061728, R37HL065619, and Fondation Leducq.

Conflicts of Interest: The authors declare no conflict of interest. The founding sponsors had no role in the design of the study; in the collection, analyses, or interpretation of data; in the writing of the manuscript, and in the decision to publish the results.

References

1. Paul, I.; Ghosh, M. K. A CHIPotle in physiology and disease. *Int. J. Biochem. Cell Biol.* **2015**, *58*, 37–52, doi:10.1016/j.biocel.2014.10.027.
2. Shi, C.-H.; Schisler, J. C.; Rubel, C. E.; Tan, S.; Song, B.; McDonough, H.; Xu, L.; Portbury, A. L.; Mao, C.-Y.; True, C.; Wang, R.-H.; Wang, Q.-Z.; Sun, S.-L.; Seminara, S. B.; Patterson, C.; Xu, Y.-M. Ataxia and hypogonadism caused by the loss of ubiquitin ligase activity of the U box protein CHIP. *Hum. Mol. Genet.* **2014**, *23*, 1013–1024, doi:10.1093/hmg/ddt497.
3. Ronnebaum, S. M.; Patterson, C.; Schisler, J. C. Emerging evidence of coding mutations in the ubiquitin–proteasome system associated with cerebellar ataxias. *Human Genome Variation* **2014**, *1*, 14018, doi:10.1038/hgv.2014.18.
4. Ronnebaum, S. M.; Patterson, C.; Schisler, J. C. Minireview: Hey U(PS): Metabolic and Proteolytic Homeostasis Linked via AMPK and the Ubiquitin Proteasome System. *Mol Endocrinol* **2014**, *28*, 1602–1615, doi:10.1210/me.2014-1180.
5. Naito, A. T.; Okada, S.; Minamino, T.; Iwanaga, K.; Liu, M.-L.; Sumida, T.; Nomura, S.; Sahara, N.; Mizoroki, T.; Takashima, A.; Akazawa, H.; Nagai, T.; Shiojima, I.; Komuro, I. Promotion of CHIP-mediated p53

degradation protects the heart from ischemic injury. *Circ. Res.* **2010**, *106*, 1692–1702, doi:10.1161/CIRCRESAHA.109.214346.

6. Le, N.-T.; Takei, Y.; Shishido, T.; Woo, C.-H.; Chang, E.; Heo, K.-S.; Lee, H.; Lu, Y.; Morrell, C.; Oikawa, M.; McClain, C.; Wang, X.; Tournier, C.; Molina, C. A.; Taunton, J.; Yan, C.; Fujiwara, K.; Patterson, C.; Yang, J.; Abe, J. p90RSK targets the ERK5-CHIP ubiquitin E3 ligase activity in diabetic hearts and promotes cardiac apoptosis and dysfunction. *Circ. Res.* **2012**, *110*, 536–550, doi:10.1161/CIRCRESAHA.111.254730.

7. Zhang, C.; Xu, Z.; He, X.-R.; Michael, L. H.; Patterson, C. CHIP, a cochaperone/ubiquitin ligase that regulates protein quality control, is required for maximal cardioprotection after myocardial infarction in mice. *Am. J. Physiol. Heart Circ. Physiol.* **2005**, *288*, H2836-2842, doi:10.1152/ajpheart.01122.2004.

8. Yang, K.; Zhang, T.-P.; Tian, C.; Jia, L.-X.; Du, J.; Li, H.-H. Carboxyl terminus of heat shock protein 70-interacting protein inhibits angiotensin II-induced cardiac remodeling. *Am. J. Hypertens.* **2012**, *25*, 994–1001, doi:10.1038/ajh.2012.74.

9. Madonna, R.; Geng, Y.-J.; Bolli, R.; Rokosh, G.; Ferdinandy, P.; Patterson, C.; De Caterina, R. Co-activation of nuclear factor-κB and myocardin/serum response factor conveys the hypertrophy signal of high insulin levels in cardiac myoblasts. *J. Biol. Chem.* **2014**, *289*, 19585–19598, doi:10.1074/jbc.M113.540559.

10. Willis, M. S.; Min, J.-N.; Wang, S.; McDonough, H.; Lockyer, P.; Wadosky, K. M.; Patterson, C. Carboxyl terminus of Hsp70-interacting protein (CHIP) is required to modulate cardiac hypertrophy and attenuate autophagy during exercise. *Cell Biochem. Funct.* **2013**, *31*, 724–735, doi:10.1002/cbf.2962.

11. Schisler, J. C.; Rubel, C. E.; Zhang, C.; Lockyer, P.; Cyr, D. M.; Patterson, C. CHIP protects against cardiac pressure overload through regulation of AMPK. *J. Clin. Invest.* **2013**, *123*, 3588–3599, doi:10.1172/JCI69080.

12. Botta, M.; Audano, M.; Sahebkar, A.; Sirtori, C. R.; Mitro, N.; Ruscica, M. PPAR Agonists and Metabolic Syndrome: An Established Role? *Int J Mol Sci* **2018**, *19*, doi:10.3390/ijms19041197.

13. Heller, F.; Harvengt, C. Effects of clofibrate, bezafibrate, fenofibrate and probucol on plasma lipolytic enzymes in normolipaemic subjects. *Eur. J. Clin. Pharmacol.* **1983**, *25*, 57–63.

14. Malmendier, C. L.; Lontie, J. F.; Delcroix, C.; Dubois, D. Y.; Magot, T.; De Roy, L. Apolipoproteins C-II and C-III metabolism in hypertriglyceridemic patients. Effect of a drastic triglyceride reduction by combined diet restriction and fenofibrate administration. *Atherosclerosis* **1989**, *77*, 139–149.

15. Martin, G.; Schoonjans, K.; Lefebvre, A. M.; Staels, B.; Auwerx, J. Coordinate regulation of the expression of the fatty acid transport protein and acyl-CoA synthetase genes by PPARalpha and PPARgamma activators. *J. Biol. Chem.* **1997**, *272*, 28210–28217.

16. Vu-Dac, N.; Schoonjans, K.; Kosykh, V.; Dallongeville, J.; Fruchart, J. C.; Staels, B.; Auwerx, J. Fibrates increase human apolipoprotein A-II expression through activation of the peroxisome proliferator-activated receptor. *J. Clin. Invest.* **1995**, *96*, 741–750, doi:10.1172/JCI118118.

17. An, J.; Muoio, D. M.; Shiota, M.; Fujimoto, Y.; Cline, G. W.; Shulman, G. I.; Koves, T. R.; Stevens, R.; Millington, D.; Newgard, C. B. Hepatic expression of malonyl-CoA decarboxylase reverses muscle, liver and whole-animal insulin resistance. *Nat. Med.* **2004**, *10*, 268–274, doi:10.1038/nm995.

18. Wu, J.-Y.; Kao, H.-J.; Li, S.-C.; Stevens, R.; Hillman, S.; Millington, D.; Chen, Y.-T. ENU mutagenesis identifies mice with mitochondrial branched-chain aminotransferase deficiency resembling human maple syrup urine disease. *J Clin Invest* **2004**, *113*, 434–440, doi:10.1172/JCI200419574.

19. Jensen, M. V.; Joseph, J. W.; Ilkayeva, O.; Burgess, S.; Lu, D.; Ronnebaum, S. M.; Odegaard, M.; Becker, T. C.; Sherry, A. D.; Newgard, C. B. Compensatory responses to pyruvate carboxylase suppression in islet beta-cells. Preservation of glucose-stimulated insulin secretion. *J. Biol. Chem.* **2006**, *281*, 22342–22351, doi:10.1074/jbc.M604350200.

20. Xia, J.; Wishart, D. S. Using MetaboAnalyst 3.0 for Comprehensive Metabolomics Data Analysis. *Curr Protoc Bioinformatics* **2016**, *55*, 14.10.1-14.10.91, doi:10.1002/cpbi.11.

21. Xia, J.; Sinelnikov, I. V.; Han, B.; Wishart, D. S. MetaboAnalyst 3.0--making metabolomics more meaningful. *Nucleic Acids Res.* **2015**, *43*, W251-257, doi:10.1093/nar/gkv380.

22. Glatz, J. F.; Veerkamp, J. H. Postnatal development of palmitate oxidation and mitochondrial enzyme activities in rat cardiac and skeletal muscle. *Biochim. Biophys. Acta* **1982**, *711*, 327–335.

23. Barger, P. M.; Brandt, J. M.; Leone, T. C.; Weinheimer, C. J.; Kelly, D. P. Deactivation of peroxisome proliferator–activated receptor-α during cardiac hypertrophic growth. *J Clin Invest* **2000**, *105*, 1723–1730.

24. Wall, S. R.; Lopaschuk, G. D. Glucose oxidation rates in fatty acid-perfused isolated working hearts from diabetic rats. *Biochim. Biophys. Acta* **1989**, *1006*, 97–103.

25. Veerkamp, J. H.; van Moerkerk, T. B.; Glatz, J. F.; Zuurveld, J. G.; Jacobs, A. E.; Wagenmakers, A. J. 14CO2 production is no adequate measure of [14C]fatty acid oxidation. *Biochem. Med. Metab. Biol.* **1986**, *35*, 248–259.
26. Rodríguez, J. E.; Liao, J.-Y.; He, J.; Schisler, J. C.; Newgard, C. B.; Drujan, D.; Glass, D. L.; Frederick, C. B.; Yoder, B. C.; Lalush, D. S.; Patterson, C.; Willis, M. S. The ubiquitin ligase MuRF1 regulates PPARα activity in the heart by enhancing nuclear export via monoubiquitination. *Mol Cell Endocrinol* **2015**, *413*, 36–48, doi:10.1016/j.mce.2015.06.008.
27. Parry, T. L.; Desai, G.; Schisler, J. C.; Li, L.; Quintana, M. T.; Stanley, N.; Lockyer, P.; Patterson, C.; Willis, M. S. Fenofibrate unexpectedly induces cardiac hypertrophy in mice lacking MuRF1. *Cardiovasc. Pathol.* **2016**, *25*, 127–140, doi:10.1016/j.carpath.2015.09.008.
28. Willis, M. S.; Rojas, M.; Li, L.; Selzman, C. H.; Tang, R.-H.; Stansfield, W. E.; Rodriguez, J. E.; Glass, D. J.; Patterson, C. Muscle ring finger 1 mediates cardiac atrophy in vivo. *Am. J. Physiol. Heart Circ. Physiol.* **2009**, *296*, H997–H1006, doi:10.1152/ajpheart.00660.2008.
29. Oakley, R. H.; Ren, R.; Cruz-Topete, D.; Bird, G. S.; Myers, P. H.; Boyle, M. C.; Schneider, M. D.; Willis, M. S.; Cidlowski, J. A. Essential role of stress hormone signaling in cardiomyocytes for the prevention of heart disease. *Proc. Natl. Acad. Sci. U.S.A.* **2013**, *110*, 17035–17040, doi:10.1073/pnas.1302546110.
30. Willis, M. S.; Dyer, L. A.; Ren, R.; Lockyer, P.; Moreno-Miralles, I.; Schisler, J. C.; Patterson, C. BMPER regulates cardiomyocyte size and vessel density in vivo. *Cardiovasc. Pathol.* **2013**, *22*, 228–240, doi:10.1016/j.carpath.2012.10.005.
31. Willis, M. S.; Schisler, J. C.; Li, L.; Rodríguez, J. E.; Hilliard, E. G.; Charles, P. C.; Patterson, C. Cardiac muscle ring finger-1 increases susceptibility to heart failure in vivo. *Circ. Res.* **2009**, *105*, 80–88, doi:10.1161/CIRCRESAHA.109.194928.
32. Colella, A. D.; Chegenii, N.; Tea, M. N.; Gibbins, I. L.; Williams, K. A.; Chataway, T. K. Comparison of Stain-Free gels with traditional immunoblot loading control methodology. *Anal. Biochem.* **2012**, *430*, 108–110, doi:10.1016/j.ab.2012.08.015.
33. Gilda, J. E.; Gomes, A. V. Stain-Free total protein staining is a superior loading control to β-actin for Western blots. *Anal. Biochem.* **2013**, *440*, 186–188, doi:10.1016/j.ab.2013.05.027.
34. A defined methodology for reliable quantification of Western blot data. - PubMed - NCBI Available online: https://www.ncbi.nlm.nih.gov/pubmed/23709336 (accessed on Jun 7, 2018).
35. Schoonjans, K.; Staels, B.; Grimaldi, P.; Auwerx, J. Acyl-CoA synthetase mRNA expression is controlled by fibric-acid derivatives, feeding and liver proliferation. *Eur. J. Biochem.* **1993**, *216*, 615–622.
36. Silvestri, E.; de Lange, P.; Moreno, M.; Lombardi, A.; Ragni, M.; Feola, A.; Schiavo, L.; Goglia, F.; Lanni, A. Fenofibrate activates the biochemical pathways and the de novo expression of genes related to lipid handling and uncoupling protein-3 functions in liver of normal rats. *Biochim. Biophys. Acta* **2006**, *1757*, 486–495, doi:10.1016/j.bbabio.2006.02.016.
37. Oosterveer, M. H.; Grefhorst, A.; van Dijk, T. H.; Havinga, R.; Staels, B.; Kuipers, F.; Groen, A. K.; Reijngoud, D.-J. Fenofibrate simultaneously induces hepatic fatty acid oxidation, synthesis, and elongation in mice. *J. Biol. Chem.* **2009**, *284*, 34036–34044, doi:10.1074/jbc.M109.051052.
38. Cattley, R. C. Regulation of cell proliferation and cell death by peroxisome proliferators. *Microsc. Res. Tech.* **2003**, *61*, 179–184, doi:10.1002/jemt.10327.
39. Declercq, V.; Yeganeh, B.; Moshtaghi-Kashanian, G.-R.; Khademi, H.; Bahadori, B.; Moghadasian, M. H. Paradoxical effects of fenofibrate and nicotinic acid in apo E-deficient mice. *J. Cardiovasc. Pharmacol.* **2005**, *46*, 18–24.
40. Schisler, J. C.; Patterson, C.; Willis, M. S. Skeletal muscle mitochondrial alterations in carboxyl terminun of HSC70 interacting protein (CHIP)$^{-/-}$ mice. *Afr J Cell Pathol* **2016**, 28–36.
41. Pascual, F.; Schisler, J. C.; Grevengoed, T. J.; Willis, M. S.; Coleman, R. A. Modeling the Transition From Decompensated to Pathological Hypertrophy. *J Am Heart Assoc* **2018**, *7*, doi:10.1161/JAHA.117.008293.
42. Schisler, J. C.; Coleman, R. A. mTORtuous effect on the elastic heart. *Oncotarget* **2015**, *6*, 16810–16811, doi:10.18632/oncotarget.4788.
43. Schisler, J. C.; Grevengoed, T. J.; Pascual, F.; Cooper, D. E.; Ellis, J. M.; Paul, D. S.; Willis, M. S.; Patterson, C.; Jia, W.; Coleman, R. A. Cardiac energy dependence on glucose increases metabolites related to glutathione and activates metabolic genes controlled by mechanistic target of rapamycin. *J Am Heart Assoc* **2015**, *4*, doi:10.1161/JAHA.114.001136.
44. Gariot, P.; Barrat, E.; Drouin, P.; Genton, P.; Pointel, J. P.; Foliguet, B.; Kolopp, M.; Debry, G. Morphometric study of human hepatic cell modifications induced by fenofibrate. *Metab. Clin. Exp.* **1987**, *36*, 203–210.

45. Guo, Y.; Jolly, R. A.; Halstead, B. W.; Baker, T. K.; Stutz, J. P.; Huffman, M.; Calley, J. N.; West, A.; Gao, H.; Searfoss, G. H.; Li, S.; Irizarry, A. R.; Qian, H.-R.; Stevens, J. L.; Ryan, T. P. Underlying mechanisms of pharmacology and toxicity of a novel PPAR agonist revealed using rodent and canine hepatocytes. *Toxicol. Sci.* **2007**, *96*, 294–309, doi:10.1093/toxsci/kfm009.

46. Nadanaciva, S.; Dykens, J. A.; Bernal, A.; Capaldi, R. A.; Will, Y. Mitochondrial impairment by PPAR agonists and statins identified via immunocaptured OXPHOS complex activities and respiration. *Toxicol. Appl. Pharmacol.* **2007**, *223*, 277–287, doi:10.1016/j.taap.2007.06.003.

47. Huang, J.; Das, S. K.; Jha, P.; Al Zoughbi, W.; Schauer, S.; Claudel, T.; Sexl, V.; Vesely, P.; Birner-Gruenberger, R.; Kratky, D.; Trauner, M.; Hoefler, G. The PPARα agonist fenofibrate suppresses B-cell lymphoma in mice by modulating lipid metabolism. *Biochim Biophys Acta* **2013**, *1831*, 1555–1565, doi:10.1016/j.bbalip.2013.04.012.

48. LeBrasseur, N. K.; Duhaney, T.-A. S.; Silva, D. S. D.; Cui, L.; Ip, P. C.; Joseph, L.; Sam, F. Effects of Fenofibrate on Cardiac Remodeling in Aldosterone-Induced Hypertension. *Hypertension* **2007**, *50*, 489–496, doi:10.1161/HYPERTENSIONAHA.107.092403.

49. Zhang, J.; Cheng, Y.; Gu, J.; Wang, S.; Zhou, S.; Wang, Y.; Tan, Y.; Feng, W.; Fu, Y.; Mellen, N.; Cheng, R.; Ma, J.; Zhang, C.; Li, Z.; Cai, L. Fenofibrate increases cardiac autophagy via FGF21/SIRT1 and prevents fibrosis and inflammation in the hearts of Type 1 diabetic mice. *Clin. Sci.* **2016**, *130*, 625–641, doi:10.1042/CS20150623.

50. Ogata, T.; Miyauchi, T.; Sakai, S.; Takanashi, M.; Irukayama-Tomobe, Y.; Yamaguchi, I. Myocardial fibrosis and diastolic dysfunction in deoxycorticosterone acetate-salt hypertensive rats is ameliorated by the peroxisome proliferator-activated receptor-alpha activator fenofibrate, partly by suppressing inflammatory responses associated with the nuclear factor-kappa-B pathway. *J. Am. Coll. Cardiol.* **2004**, *43*, 1481–1488, doi:10.1016/j.jacc.2003.11.043.

51. Dhahri, W.; Couet, J.; Roussel, É.; Drolet, M.-C.; Arsenault, M. Fenofibrate reduces cardiac remodeling and improves cardiac function in a rat model of severe left ventricle volume overload. *Life Sci.* **2013**, *92*, 26–34, doi:10.1016/j.lfs.2012.10.022.

52. Labinskyy, V.; Bellomo, M.; Chandler, M. P.; Young, M. E.; Lionetti, V.; Qanud, K.; Bigazzi, F.; Sampietro, T.; Stanley, W. C.; Recchia, F. A. Chronic activation of peroxisome proliferator-activated receptor-alpha with fenofibrate prevents alterations in cardiac metabolic phenotype without changing the onset of decompensation in pacing-induced heart failure. *J. Pharmacol. Exp. Ther.* **2007**, *321*, 165–171, doi:10.1124/jpet.106.116871.

53. Li, C.-B.; Li, X.-X.; Chen, Y.-G.; Zhang, C.; Zhang, M.-X.; Zhao, X.-Q.; Hao, M.-X.; Hou, X.-Y.; Gong, M.-L.; Zhao, Y.-X.; Bu, P.-L.; Zhang, Y. Effects and mechanisms of PPARalpha activator fenofibrate on myocardial remodelling in hypertension. *J. Cell. Mol. Med.* **2009**, *13*, 4444–4452, doi:10.1111/j.1582-4934.2008.00484.x.

54. Duhaney, T.-A. S.; Cui, L.; Rude, M. K.; Lebrasseur, N. K.; Ngoy, S.; De Silva, D. S.; Siwik, D. A.; Liao, R.; Sam, F. Peroxisome proliferator-activated receptor alpha-independent actions of fenofibrate exacerbates left ventricular dilation and fibrosis in chronic pressure overload. *Hypertension* **2007**, *49*, 1084–1094, doi:10.1161/HYPERTENSIONAHA.107.086926.

55. Punthakee, Z.; Scully, L. J.; Guindi, M. M.; Ooi, T. C. Liver fibrosis attributed to lipid lowering medications: two cases. *J. Intern. Med.* **2001**, *250*, 249–254.

56. Attridge, R. L.; Frei, C. R.; Ryan, L.; Koeller, J.; Linn, W. D. Fenofibrate-associated nephrotoxicity: a review of current evidence. *Am J Health Syst Pharm* **2013**, *70*, 1219–1225, doi:10.2146/ajhp120131.

57. Olivé, M.; Abdul-Hussein, S.; Oldfors, A.; González-Costello, J.; van der Ven, P. F. M.; Fürst, D. O.; González, L.; Moreno, D.; Torrejón-Escribano, B.; Alió, J.; Pou, A.; Ferrer, I.; Tajsharghi, H. New cardiac and skeletal protein aggregate myopathy associated with combined MuRF1 and MuRF3 mutations. *Hum. Mol. Genet.* **2015**, *24*, 3638–3650, doi:10.1093/hmg/ddv108.

58. Su, M.; Wang, J.; Kang, L.; Wang, Y.; Zou, Y.; Feng, X.; Wang, D.; Ahmad, F.; Zhou, X.; Hui, R.; Song, L. Rare variants in genes encoding MuRF1 and MuRF2 are modifiers of hypertrophic cardiomyopathy. *Int J Mol Sci* **2014**, *15*, 9302–9313, doi:10.3390/ijms15069302.

59. Bosman, F. T.; Stamenkovic, I. Functional structure and composition of the extracellular matrix. *J. Pathol.* **2003**, *200*, 423–428, doi:10.1002/path.1437.

60. Zhang, P.; Su, J.; Mende, U. Cross talk between cardiac myocytes and fibroblasts: from multiscale investigative approaches to mechanisms and functional consequences. *Am. J. Physiol. Heart Circ. Physiol.* **2012**, *303*, H1385-1396, doi:10.1152/ajpheart.01167.2011.

61. Rother, J.; Richter, C.; Turco, L.; Knoch, F.; Mey, I.; Luther, S.; Janshoff, A.; Bodenschatz, E.; Tarantola, M. Crosstalk of cardiomyocytes and fibroblasts in co-cultures. *Open Biol* **2015**, *5*, 150038, doi:10.1098/rsob.150038.

587 62. Lyu, L.; Wang, H.; Li, B.; Qin, Q.; Qi, L.; Nagarkatti, M.; Nagarkatti, P.; Janicki, J. S.; Wang, X. L.; Cui, T. A
588 critical role of cardiac fibroblast-derived exosomes in activating renin angiotensin system in cardiomyocytes. *J.*
589 *Mol. Cell. Cardiol.* **2015**, *89*, 268–279, doi:10.1016/j.yjmcc.2015.10.022.
590 63. Yoon, P. O.; Lee, M.-A.; Cha, H.; Jeong, M. H.; Kim, J.; Jang, S. P.; Choi, B. Y.; Jeong, D.; Yang, D. K.; Hajjar,
591 R. J.; Park, W. J. The opposing effects of CCN2 and CCN5 on the development of cardiac hypertrophy and
592 fibrosis. *J. Mol. Cell. Cardiol.* **2010**, *49*, 294–303, doi:10.1016/j.yjmcc.2010.04.010.
593 64. Nishida, M.; Sato, Y.; Uemura, A.; Narita, Y.; Tozaki-Saitoh, H.; Nakaya, M.; Ide, T.; Suzuki, K.; Inoue, K.;
594 Nagao, T.; Kurose, H. P2Y6 receptor-Galpha12/13 signalling in cardiomyocytes triggers pressure overload-
595 induced cardiac fibrosis. *EMBO J.* **2008**, *27*, 3104–3115, doi:10.1038/emboj.2008.237.